Polarization fading mitigation in distributed acoustic sensors based on a high-speed polarization rotator

SHAHAB BAKHTIARI GORAJOOBI*, ALI MASOUDI, GILBERTO BRAMBILLA

Optoelectronics Research Centre, University of Southampton, Southampton, SO17 1BJ, UK

**Corresponding author: sbq1v17@soton.ac.uk*

Received XX Month XXXX; revised XX Month, XXXX; accepted XX Month XXXX; posted XX Month XXXX (Doc. ID XXXXX); published XX Month XXXX

A distributed optical fiber acoustic sensor based on interferometric demodulation technique with no polarization fading is demonstrated. A polarization diversity scheme based on high-speed polarization rotator is used to eliminate signal fading due to polarization mismatch in the Rayleigh backscattered signal between adjacent points on the sensing fiber. This technique yields a spatially uniform response to the applied strain. The sensor exhibited a spatial and strain resolutions of 4m and < 3nε, respectively, over a sensing range of 8.5km. © 2020 Optica Publishing Group

Phase-sensitive Optical Time-domain Reflectometry (ϕ-OTDR) enables quantification of dynamic strains along an optical fiber by analyzing the phase of the Rayleigh backscattered light from an optical pulse launched into the fiber [1]. Such technology forms the basis of Distributed Acoustic Sensors (DASs), which are employed to monitor pipelines, cables, infrastructures and seismic events [2-7]. Measurement fidelity of DASs has increased in importance as industries progressively demanded systems with improved range, resolution, and sensitivity. Signal fading, as one of the hallmarks of interferometric DAS systems, plays an adverse role in the measurement fidelity.

DASs suffer from three types of signal fading: intensity, phase, and polarization fading. Intensity fading happens when the backscattered electromagnetic waves from inhomogeneities at a given section of the sensing fiber are destructively added to one another reducing the intensity of the backscattered light from that section to a level close to zero. Phase fading occurs when the phase-difference between the backscattered lights from two segments on the fiber, separated by the gauge length, is an integer multiple of π. In such scenario, where the superposition of the backscattered signals is at a maxima or minima of the interferometric pattern, a small strain variation over the said gauge length results in minute intensity changes at the output of the interferometer which, in turn, translates into signal fading. Finally, polarization fading occurs when the polarization of backscattered lights from two ends of the said gauge length are orthogonal. Since lights with orthogonal polarizations do not mix, no interferometric pattern is formed at the output of the interferometer which, subsequently, results in signal fading.

To eliminate intensity fading, Hartog et al. proposed a frequency diversity interrogation technique [8], in which the frequency of the seed laser is up-shifted in several steps to create several statistically independent Rayleigh backscattered traces with different coherent Rayleigh noise patterns. By combining the measurements from the Rayleigh backscattered traces acquired at different frequencies, it is possible to eliminate the intensity fading while increasing the sensing precision, albeit at the cost of reduced measurement bandwidth. All other coherent DAS systems that have been developed to eliminate intensity fading are based on the same concept, but with different implementations [9-13].

Techniques adopted for eliminating phase fading are tailored to the DAS sensing approach [2, 14]. Interferometric DAS systems, for instance, use two approaches: 1) a 3×3 coupler to create three signals 2π/3 out of phase [15, 16] and 2) phase generated carrier which relies on the modulation of the phase of light in one arm of the interferometer and its mixture with the light from the other arm to generate a beat frequency [17, 18]. For dual-pulse DAS systems, the phase fading has been eliminated by shifting the phase difference between subsequent pulse-pairs by 2π/3, but at the cost of reduced measurement bandwidth [19]. For coherent DAS systems, the most used technique is based on a 90° hybrid [20-22].

Polarization fading is less of an issue for the majority of DAS applications, especially those relying on a straight Single Mode Fibers (SMFs) with a relatively low birefringence over the gauge length of the DAS system [3, 23-25]. However, for applications that are based on wounded fibers such as distributed optical fiber hydrophones [26] or helically wound fiber optic cables such as vertical seismic profiling [27], polarization fading might result in a substantial signal fading. So far, only coherent DAS systems have addressed polarization fading through polarization diversity detection [21, 28]. In this technique, a polarization beam splitter is used to split the backscattered light into two orthogonal polarizations and the phase information at each State of Polarization (SoP) is obtained through coherent detection. Polarization diversity approach, however, requires twice as many balance detectors (the total of four balanced detectors in the case of

dual polarization 90° hybrid) and may yield lower SNR due to the additional losses from the addition of polarization beam splitter.

In this letter, a new sensing arrangement based on a high-speed polarization rotator is used to mitigate polarization fading in an interferometric DAS system. The polarization rotator is added in one arm of an imbalanced Mach-Zehnder Interferometer (IMZI) to rotate the polarization of the light in one arm of the interferometer between two orthogonal states before mixing it with the light in the other arm. The implementation of polarization diversity scheme has yielded a more uniform strain measurement with lower signal distortion and better strain accuracy.

The sensing principle of an interferometric DAS with polarization diversity provision is, for most part, similar to that of a conventional interferometric DAS. In conventional interferometric DAS, the dynamic strain at any given section of the sensing fiber is measured by mixing the backscattered light from the two ends of that section and evaluating the variation in the phase of the mixed light [15]. To mix the light from different points on the fiber that are separated by the gauge length, an IMZI with a path-different twice that of the gauge length is used. However, since the birefringence induced by fiber imperfections changes the polarization state of the light, there might be sections along the sensing fiber, separated by the gauge length, where the backscattered signals do not mix properly and causing signal fading (Fig. 1(a)). To address this issue, a polarization rotator can be incorporated in the IMZI to sequentially rotate the polarization of the light in one arm of the interferometer between 0° and 180° before combining it with the light from the other arm (Fig. 1(b)). By adopting this sensing arrangement, it can be guaranteed

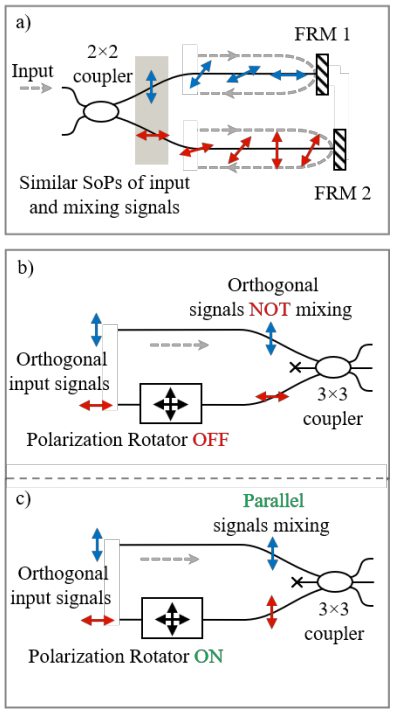

Fig. 1. a) Schematic of a MI demodulation technique using Faraday Rotating Mirrors (FRMs) suffering from polarization fading when signals with orthogonal polarizations enter the two arms of the interferometer and mix with the same polarizations state at the output 2×2 coupler, and demonstration of a MZI demodulation technique based on a polarization rotator at b) off, and c) on states eliminating polarization fading at the output 3×3 coupler.

that the light from any given points on the fiber that are separated

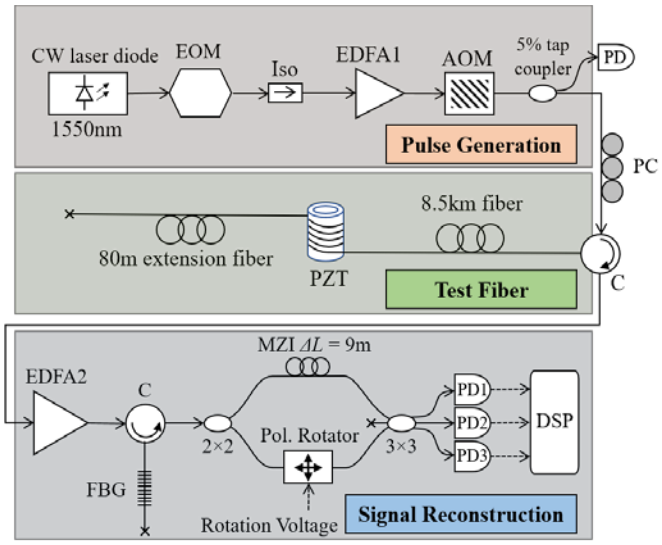

Fig. 2. Experimental setup. CW: Continuous-wave, EOM: Electro-optic Modulator, EDFA: Erbium-doped fiber amplifier, AOM: Acousto-optic Modulator, PC: Polarization Controller, C: Circulator, PZT: Piezoelectric Transducer, FBG: Fiber Bragg Grating, MZI: Mach Zehnder Interferometer, PD: Photodetector.

by the gauge length will be mixed with one another. Hence, by combining the data from two SoP through, for instance, calculating the weighted average of the data obtained from two polarization states, the polarization fading can be eliminated.

It should be noted that interferometric DAS systems that use Michelson Interferometer (MI) at their receiving arm are still susceptible to polarization fading [16-18]. As schematically shown in Fig. 1(c), MI does not address the polarization fading issue that may occur due to orthogonal SoP of the backscattered lights. A MI can only eliminate polarization fading within the interferometer.

The experimental setup used in this study is shown in Fig. 2. A 1550nm Continuous-wave (CW) laser diode with 10mW mean power is intensity modulated by an Electro-optic Modulator (EOM) to generate 40ns pulses at a repetition frequency of 10kHz. Each pulse passes through an optical isolator and then amplified using an Erbium-doped Fiber Amplifier (EDFA1). An Acousto-optic Modulator (AOM) with >50dB extinction ratio is used to eliminate the Amplified Spontaneous Emission (ASE) of the EDFA1. A tap coupler is employed to monitor the pulse power and profile. The SoP of the pulse entering the test fiber is altered using a polarization controller to stimulate polarization states that induce signal fading. The probe pulse with 145mW peak power is launched into the test fiber via circulator C1. The test fiber includes 8.5km of SMF Corning SMF-28) spliced to 1.7m of fiber wound around a Piezoelectric Transducer (PZT) with an outer diameter of 38mm. An 80m long SMF is added to the fibre on the PZT to separate to separate the test region from the far-end of the sensing fiber. The optical circulator C1 directs the backscattered light into the receiving arm of the setup. At this stage, EDFA2 amplifies the signal which is then filtered using a Fiber Bragg Grating (FBG) filter with a reflectivity and bandwidth of 59% and 0.03nm, respectively. A MZI with a path imbalance of ΔL = 9m is adapted to accommodate a polarization rotator in one of its arms. A symmetric 3×3 coupler is spliced to the two arms of the MZI at one end and to three Photodetectors (PDs) with 125MHz bandwidth at the other end [29]. A digitizer with

500MHz bandwidth acquires the output voltages of the PDs.

The polarization rotator is programmed to shift the SoP of the light in one arm of the interferometer by 180° on the Poincare Sphere for every other backscattered traces. Figures 3(a) and 3(b) show a schematic plot of the OTDR traces and the switching sequence of the polarization rotator. A demodulation scheme based on arctangent function is used to extract the phase information from the Rayleigh backscattered traces [15].

The polarization rotator performs as a variable quarter-wave plate retarder. Such that, in case of a pure linearly-polarized light, it rotates the SoP of the field to the corresponding orthogonal one. Figure 4(a) plots the response of the polarization rotator to a light wave with an arbitrary initial SoP of *s* on the Poincarè sphere, where S1-S3 denote the Stokes parameters in cartesian coordinates. For any point on the Poincarè sphere, the polarization rotator transforms the SoP to its corresponding diametrical point on the circle of rotation. Figure 4(b) shows the backscattered traces at the output of the MZI obtained at OFF (blue trace) and ON (orange trace) state of the polarization rotator along a 110m- section of the test fiber. The two traces show that the polarization of the backscattered Rayleigh light at the output of the MZI can have near orthogonal polarizations which can cause polarization fading. At other positions, no significant fading can be observed due to presence of non-orthogonal polarization components in the combined waves.

To implement the polarization diversity scheme shown in Fig. 3, the OTDR traces with the same SoP are analyzed together. This reduces the effective sampling rate of the sensor by a factor of two down to 5kHz. Figure 5 plots the response of the DAS system to a sinusoidal strain wave imposed on a sensing fiber interrogated by a probe pulses with three different SoPs. The amplitude and frequency of the strain wave was set to 1με and 10Hz, respectively,. Figures 5(a) and 5(b) show the output of the DAS at two states of the polarization rotator. The Fast Fourier Transforms (FFTs) of both waterfall plots are shown in Fig. 5(c), showing no significant discrepancy between the results obtained before and after polarization rotation. A weighted average of both results was used to calculate the strain. The reconstructed phase, $\Delta\phi(s,p)$, can be obtained from the phases of individual traces, $\Delta\phi(s)$ and $\Delta\phi(p)$ for *s* and *p* SoPs, respectively, such that

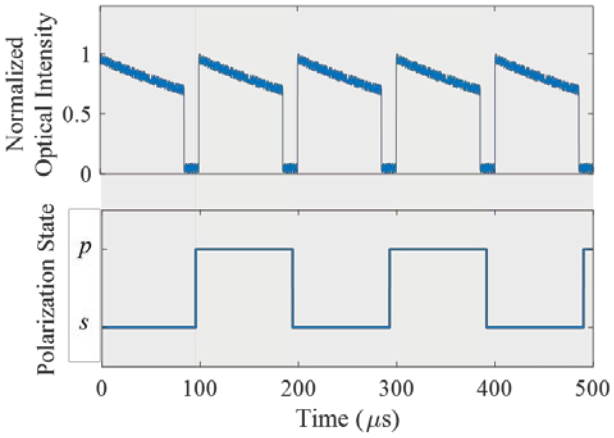

Fig. 3. Schematic of (a) OTDR traces, and (b) corresponding polarization sate of the polarization rotator.

$$\Delta\phi(s,p)=\frac{FFT(s)\times\Delta\phi(s)+FFT(p)\times\Delta\phi(p)}{FFT(s)+FFT(p)} \quad (1)$$

where *FFT*(*s*) and *FFT*(*p*) denote the amplitude of FFTs at *s* and *p* SoPs, respectively. Figure 5(d) shows the reconstructed data using Eq. (1). For the first dataset, the reconstructed data does not show any improvement compared to the single polarization cases shown in Figs. 5(a) and 5(b). This shows that there was no polarization

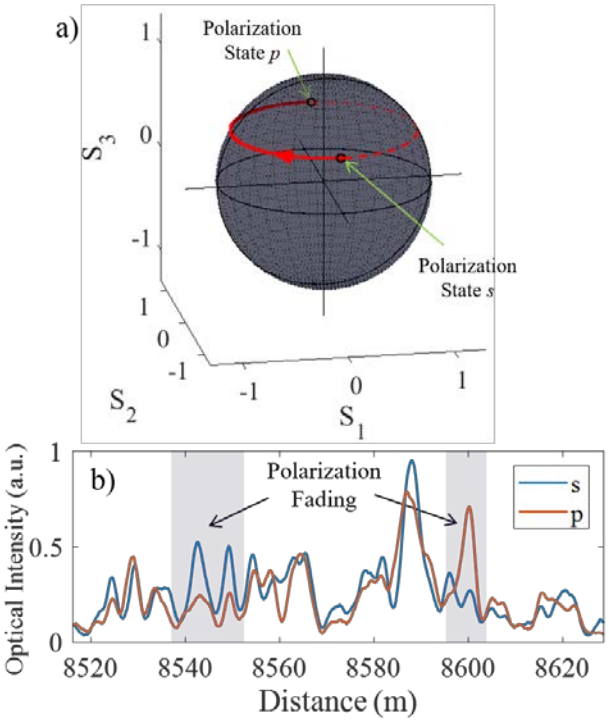

Fig. 4. (a) Example of the performance of the polarization rotator form the polarimetry experiment when an arbitrary SoP of *s* on the Poincarè sphere is rotated to the antipodal point resulted in SOP of *p* (solid red line), and (b) The OTDR traces at the end of the test fiber corresponding to the two SoPs of *s* and *p* showing the polarization fading effect can occur at certain positions along the fiber.

fading at the output of the MZI for the SoP of the probe pulse used to obtain the first dataset. When the polarization of the probe pulse was changed using the polarization controller in Fig. 2, the visibility of the signal was deteriorated at few points along the sensing fiber due to polarization fading. The experimental results from 2nd and 3rd data sets, plotted respectively in Figs. 5(e-h) and 5(i-l), demonstrate such cases. Data set 2 shows that the signal fades at selected positions along the fiber for both *s* and *p* SoPs (noticeably at 8622m in Fig. 5(e) and 8620m in Fig. 5(f)), whereas data set 3 exhibits signal fading only for the *p* SoP (see Figs. 5(i) and 5(j) at 8620m). The reconstructed signals for both cases, plotted in Figs. 5(h) and 5(l), show a uniform response along the sensing fiber where the strain is applied with no significant signal distortion. A 2D cross-section of the response of the sensor at 8620m for data set 3 is plotted in Fig. 6. Results show that the reconstructed signal from both *s* and *p* SoPs has a greater amplitude compared to the *p* SoP which suffers from signal distortion due to polarization fading. In this study, to induce high birefringence, the test fiber was wound around a PZT with an outer diameter of 38mm.

In summary, a DAS system based on a polarization diversity scheme was developed. Polarization diversity was achieved by embedding a high-speed polarization rotator in one arm of the MZI, which

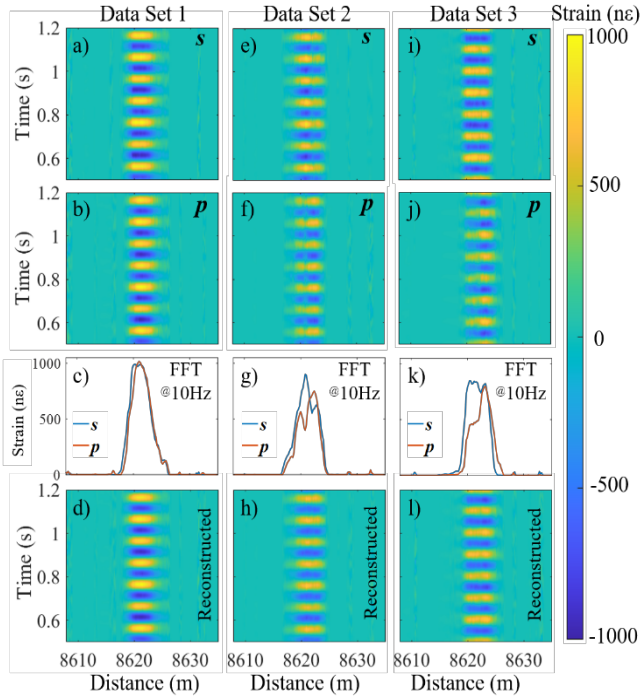

Fig. 5. Characterization of the DAS sensor using a sinusoidal strain wave with frequency and amplitude of 10 Hz and 1με for three cases. 1) data set 1: no polarization fading at both (a) *s*, and (b) *p* polarization switching states, (c) corresponding FFTs, and (d) reconstructed signal using a weighted average; 2) data set 2: polarization fading at both (e) *s*, and (f) *p* states, (g) corresponding FFTs, and (h) reconstructed signal; and 3) data set 3: no polarization fading at (i) *s* state, but polarization fading at (j) *p* state, (k) corresponding FFTs, and (l) reconstructed signal.

rotated the SoP of the light by 180° on the Poincarè sphere. Experimental results showed that when polarization fading occurs for either rotated or unrotated SoPs, a weighted average of the data obtain at both signals can be used to improve the measurement precision of the sensor. The sensor had 4m spatial resolution, 5kHz sampling rate, and 8.5km sensing range. Strain variations at the frequency of 10Hz were measured with an accuracy of < 3nε. This method can be used in conjunction with frequency diversity scheme to eliminate all signal fadings in a DAS system.

Funding. Royal Society (CHL/R1/180350); Natural Environment Research Council (NE/S012877/1, NE/T005890/1).

Disclosures. The authors declare no conflicts of interest.

References

1. A. Masoudi, M. Belal, and T. P. Newson, "A distributed optical fibre dynamic strain sensor based on phase-OTDR," Measurement Science and Technology **24**(8), 085204 (2013).
2. A. Masoudi, and T. P. Newson, "Contributed Review: Distributed optical fibre dynamic strain sensing," Rev Sci Instrum **87**(1), 011501 (2016).
3. A. Masoudi, J. A. Pilgrim, T. P. Newson, and G. Brambilla, "Subsea Cable Condition Monitoring With Distributed Optical Fiber Vibration Sensor," Journal of Lightwave Technology **37**(4), 1352-1358 (2019).
4. Z. W. Ding, X. P. Zhang, N. M. Zou, F. Xiong, J. Y. Song, X. Fang, F. Wang, and Y. X. Zhang, "Phi-OTDR Based On-Line Monitoring of Overhead Power Transmission Line," Journal of Lightwave Technology **39**(15), 5163-5169 (2021).
5. A. Lellouch, and B. L. Biondi, "Seismic Applications of Downhole DAS," Sensors (Basel) **21**(9), 2897 (2021).

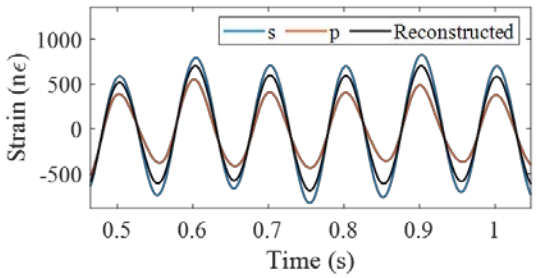

Fig. 6 A 2D cross-sectional view of data set 3 at 8620m showing the measured strain as a function of time for *s* and *p* SoPs as well as the reconstructed signal.

6. R. Law, P. Christoffersen, B. Hubbard, S. H. Doyle, T. R. Chudley, C. M. Schoonman, M. Bougamont, B. d. Tombe, B. Schilperoort, C. Kechavarzi, A. Booth, and T. J. Young, "Thermodynamics of a fast-moving Greenlandic outlet glacier revealed by fiber-optic distributed temperature sensing," Science Advances **7**(20), eabe7136 (2021).
7. T. S. Hudson, A. F. Baird, J. M. Kendall, S. K. Kufner, A. M. Brisbourne, A. M. Smith, A. Butcher, A. Chalari, and A. Clarke, "Distributed Acoustic Sensing (DAS) for Natural Microseismicity Studies: A Case Study From Antarctica," Journal of Geophysical Research: Solid Earth **126**(7) (2021).
8. A. H. Hartog, L. B. Liokumovich, N. A. Ushakov, O. I. Kotov, T. Dean, T. Cuny, A. Constantinou, and F. V. Englich, "The use of multi - frequency acquisition to significantly improve the quality of fibre - optic - distributed vibration sensing," Geophysical Prospecting **66**(S1), 192-202 (2018).
9. Y. Hu, Z. Meng, M. Zabihi, Y. Shan, S. Fu, F. Wang, X. Zhang, Y. Zhang, and B. Zeng, "Performance Enhancement Methods for the Distributed Acoustic Sensors Based on Frequency Division Multiplexing," Electronics **8**(6), 617 (2019).
10. S. Lin, Z. Wang, J. Xiong, Y. Fu, J. Jiang, Y. Wu, Y. Chen, C. Lu, and Y. Rao, "Rayleigh Fading Suppression in One-Dimensional Optical Scatters," IEEE Access **7**(17125-17132 (2019).
11. J. Gu, B. Lu, J. Yang, Z. Wang, L. Ye, Q. Ye, R. Qu, and H. Cai, "High SNR Φ-OTDR Based on Frequency and Wavelength Diversity With Differential Vector Aggregation Method," IEEE Photonics Journal **12**(6), 1-12 (2020).
12. M. Zabihi, Y. Chen, T. Zhou, J. Liu, Y. Shan, Z. Meng, F. Wang, Y. Zhang, X. Zhang, and M. Chen, "Continuous Fading Suppression Method for Φ-OTDR Systems Using Optimum Tracking Over Multiple Probe Frequencies," Journal of Lightwave Technology **37**(14), 3602-3610 (2019).
13. H. M. Ogden, M. J. Murray, J. B. Murray, C. Kirkendall, and B. Redding, "Frequency multiplexed coherent phi-OTDR," Sci Rep **11**(1), 17921 (2021).
14. Y. Rao, Z. Wang, H. Wu, Z. Ran, and B. Han, "Recent Advances in Phase-Sensitive Optical Time Domain Reflectometry (Φ-OTDR)," Photonic Sensors **11**(1), 1-30 (2021).
15. A. Masoudi, and T. P. Newson, "High spatial resolution distributed optical fiber dynamic strain sensor with enhanced frequency and strain resolution," Opt Lett **42**(2), 290-293 (2017).
16. C. Wang, C. Wang, Y. Shang, X. Liu, and G. Peng, "Distributed acoustic mapping based on interferometry of phase optical time-domain reflectometry," Optics Communications **346**(172-177 (2015).
17. G. Fang, T. Xu, S. Feng, and F. Li, "Phase-Sensitive Optical Time Domain Reflectometer Based on Phase-Generated Carrier Algorithm," Journal of Lightwave Technology **33**(13), 2811-2816 (2015).
18. Z. Yu, Q. Zhang, M. Zhang, H. Dai, J. Zhang, L. Liu, L. Zhang, X. Jin, G. Wang, and G. Qi, "Distributed optical fiber vibration sensing using phase-generated carrier demodulation algorithm," Applied Physics B **124**(5) (2018).
19. A. E. Alekseev, V. S. Vdovenko, B. G. Gorshkov, V. T. Potapov, and D. E. Simikin, "A phase-sensitive optical time-domain reflectometer with dual-pulse phase modulated probe signal," Laser Physics **24**(11) (2014).

20. Z. Wang, L. Zhang, S. Wang, N. Xue, F. Peng, M. Fan, W. Sun, X. Qian, J. Rao, and Y. Rao, "Coherent Phi-OTDR based on I/Q demodulation and homodyne detection," Opt Express **24**(2), 853-858 (2016).
21. J. J. Mompo, L. Shiloh, N. Arbel, N. Levanon, A. Loayssa, and A. Eyal, "Distributed Dynamic Strain Sensing via Perfect Periodic Coherent Codes and a Polarization Diversity Receiver," Journal of Lightwave Technology **37**(18), 4597-4602 (2019).
22. Y. Wakisaka, D. Iida, H. Oshida, and N. Honda, "Fading Suppression of Φ-OTDR With the New Signal Processing Methodology of Complex Vectors Across Time and Frequency Domains," Journal of Lightwave Technology **39**(13), 4279-4293 (2021).
23. D. Milne, A. Masoudi, E. Ferro, G. Watson, and L. Le Pen, "An analysis of railway track behaviour based on distributed optical fibre acoustic sensing," Mechanical Systems and Signal Processing **142**(106769 (2020).
24. N. J. Lindsey, and E. R. Martin, "Fiber-Optic Seismology," Annual Review of Earth and Planetary Sciences **49**(1), 309-336 (2021).
25. D. Rivet, B. de Cacqueray, A. Sladen, A. Roques, and G. Calbris, "Preliminary assessment of ship detection and trajectory evaluation using distributed acoustic sensing on an optical fiber telecom cable," J Acoust Soc Am **149**(4), 2615 (2021).
26. B. Lu, B. Wu, J. Gu, J. Yang, K. Gao, Z. Wang, L. Ye, Q. Ye, R. Qu, X. Chen, and H. Cai, "Distributed optical fiber hydrophone based on Phi-OTDR and its field test," Opt Express **29**(3), 3147-3162 (2021).
27. B. N. Kuvshinov, "Interaction of helically wound fibre-optic cables with plane seismic waves," Geophysical Prospecting **64**(3), 671-688 (2016).
28. C. Dorize, S. Guerrier, E. Awwad, and J. Renaudier, "Identification of Rayleigh fading induced phase artifacts in coherent differential varphi-OTDR," Opt Lett **46**(11), 2754-2757 (2021).
29. M. Chen, A. Masoudi, and G. Brambilla, "Performance analysis of distributed optical fiber acoustic sensors based on phi-OTDR," Opt Express **27**(7), 9684-9695 (2019).